

Chapter 5

What Do Contact Angles Measure?

Abstract Contact angle measurement has widely been used to characterize the properties of solid surfaces and study liquid–surface interactions. It has been known for some time that, while the measurement itself is deceptively simple, the interpretation is not straightforward and can be very complex. Correlations between contact angle data (static contact angle θ , advancing and receding contact angle θ_A and θ_R , hysteresis ($\theta_A - \theta_R$), and sliding angle α) and surface wettability and adhesion are at times confusing. In an attempt to find out what surface properties contact angles are measuring, Samuel, Zhao, and Law systematically measure the wetting and adhesion forces between water and 20 surfaces and correlate them with contact angle data. The surface properties of the 20 surfaces vary from hydrophilic to hydrophobic to superhydrophobic, and their morphology varies from atomic smooth to homogeneously rough in the nano- and micron scale. Based on the good correlations found between θ_A and the wetting force and θ_R with the adhesion force, it was concluded that θ_A and θ_R are measures of surface wettability and adhesion, respectively. Since sliding angle α is a measure of drop mobility, it is recommended that surface should be characterized by their wettability, adhesion and stickiness using θ_A , θ_R , and α , respectively. As for contact angle hysteresis, the analysis suggests that it is a measure of the difference in liquid–surface interfacial tension during advancing and during receding. The use of the basic concepts described in this chapter to comprehend properties displayed by some recently reported unconventional surfaces is discussed. These unconventional surfaces are surfaces with very large contact angles but very sticky or with small contact angles and very slippery.

Keywords Contact angle measurement • Static contact angle • Advancing contact angle • Receding contact angle • Sliding angle • Contact angle hysteresis • Liquid–solid interactions • Data interpretation • Wetting interaction • Adhesion interaction • Young–Dupre equation • Contact angle hysteresis mechanism

5.1 Background

Since the report of the angle of contact between a liquid droplet and a solid surface by Thomas Young more than two centuries ago [1], there has been continuous arguments in the literature regarding the validity of the Young’s angle and how it may be used to study surface and liquid–surface interactions. The Young’s angle by itself is

problematic because it consists of four quantities and two of which cannot be measured reliably. The observation of the advancing and receding contact angle in addition to the Young's angle by Rayleigh [2] and later confirmed by Bartell and coworkers [3, 4] fired up the conversation further. Researchers in the nineteenth century were strongly influenced by the thermodynamic approaches put forwarded by Dupre [5] and Gibbs [6]. As pointed out by Shuttleworth and Bailey [7] in 1948, thermodynamic (free energy) is only part of the contributor for the Young's angle during liquid wetting. This point was recognized [8] but not well understood in the literature. In view of the observation of three contact angles (static contact angle θ and advancing and receding contact angle θ_A and θ_R), some researchers created the term "ideal" surface for surfaces that are smooth, rigid, and has zero hysteresis, $\theta_A = \theta_R$. The rest, including rough and smooth heterogeneous surfaces, would be the "real" surfaces. Some believed that hysteresis is a result of defect or heterogeneity or roughness [9]. Good [10] advocated strongly that authors should either report both θ_A and θ_R or a static contact angle (θ) along with the hysteresis value ($\theta_A - \theta_R$), otherwise journals should not published these papers. The arguments seem endless and remain unsettled to date. Given this backdrop, misperceptions, such as (a) non-stickiness is a result of a large contact angle, (b) surface adhesion is due to contact angle hysteresis, or (c) contact angle θ is related to both wettability and adhesion, have been reported [11–14]. Our primary intention here is to make readers aware of the key debates, while sparing the details of all past arguments. We feel that a detailed account of all the arguments would create more harm and confusion than good. Rather, we are looking forward and articulate the basic surface concepts that are needed to advance the science for surfaces in the future.

Now let's take a step back and ask ourselves a simple question. Why are we interested in contact angle measurement? The short answer is that contact angle measurement is a very simple measurement tool for surface science. The measured contact angle is known to provide insight about surface properties as well as how liquid and surface interact, such as wetting, spreading, adhesion, and evaporation. Unfortunately, due to the difficulty in interpreting contact angle data, the literature often consists of controversial and sometimes conflicting messages. For example, the use of water as a probing liquid is very common, and surfaces with large water contact angles are highly hydrophobic, and they are usually lower in surface energy [15–17]. What's not well recognized is that large water contact angle and low surface energy may not be correlating to both wettability and adhesion simultaneously [18–21]. Tsai, Chou, and Penn [19] reported the lack of correlation between contact angle data and the adhesive performance for the smooth surfaces on a series of Kevlar fiber. Murase and Fujibayashi [20] found that while the surface of their fluorinated polymer exhibit a larger water contact angle (117°) than that of the polydimethylsiloxane sample (102°), the interactive energy with water for the fluoropolymer is three times higher (~ 50.89 versus 15.64 mJ/m^2). Silicones and fluoropolymers, e.g., Teflon (PTFE), are two classes of well-known low-surface-energy materials that are frequently used in the fusing components in the printing industry [22, 23]. Both materials are highly hydrophobic with PTFE having a slightly larger water contact angle than PDMS silicone (112 – 117° for PTFE as compared to 102 – 103° for PDMS). However, PTFE was consistently shown to adhere stronger to water and

has a larger sliding angle [20, 21]. To an extreme, Gao and McCarthy [24] even called Teflon hydrophilic. The fundamental question we have to ask is: what does contact angle mean to surface attraction and adhesion? Are these interactive forces in any way correlating to the surface properties? These questions are not new. They had been asked before and remained to be clarified [25]. With the advance of modern instrumentation, we thought if liquid–surface interactions can be measured directly and independently, a study of how liquid–surface interactions are correlating to the different contact angles would be useful and interesting. It is our hope that examination of these correlations or trends would shine light on the true meaning of each contact angle measurement.

5.2 Contact Angles and Liquid–Solid Interactions

5.2.1 Contact Angles

The most common properties for surfaces are their wettability and adhesion. Wettability is used to describe the interaction when a liquid first makes contact to a solid surface. On the other hand, adhesion is a description of the force when a liquid is separating from a solid surface. These are two very different interactions, yet contact angles have been used to study and correlate both [25]. Therefore, it comes no surprise that controversial and conflicting findings exist. To find out what contact angles are measuring, Samuel, Zhao, and Law [26] recently launched a systematic study involving measurements of all the contact angles for a series of surfaces and correlating them with measurable forces derived from wetting and adhesion. Water was chosen as the probing liquid. The static and dynamic contact angles (θ , θ_A , θ_R , and sliding angle α) and contact angle hysteresis on 20 different surfaces (1–20) were determined. The data are summarized in Table 5.1. These 20 surfaces were cleaned appropriately prior to all contact angle measurements. They represent surfaces of all traits. Their affinity toward water varies from hydrophilic to hydrophobic to superhydrophobic. Their surface morphology varies from atomic smooth (self-assembled monolayers or CVD films on silicon wafer, 7–11) to films from blade coating (1–3, 6, 13) to commercial plastic films (4, 5, 12, 14) to photolithographic textured surfaces (15–18) to rough surfaces from nature (19, 20). Figures 5.1, 5.2, and 5.3 plot the static contact angle θ against sliding angle α , contact angle hysteresis ($\theta_A - \theta_R$), and ($\cos\theta_R - \cos\theta_A$), respectively.

In the literature, sliding angle and contact angle hysteresis have been thought to be related to surface stickiness and adhesion. The larger the sliding angle, the stickier the surface; the larger the contact angle hysteresis, the stronger the surface adhesion. Now, if one considers all 20 surfaces, flat, smooth, rough, and textured, the data points are very scattered. The results lead to the general conclusion that, there is no correlation between static contact angle θ and surface stickiness or adhesion. Although similar conclusions have been reached earlier [15, 16, 19, 20], the lack of correlation observed by Samuel, Zhao, and Law [26] is still significant because the study comprised of a very wide range of surfaces, implying that the noncorrelation is genuine.

Table 5.1 Contact angle measurement data and wetting and adhesion force data for water on different surfaces (data from [26])

No	Polymer surfaces	θ^a	θ_A^b	θ_R^c	α^d	$(\theta_A - \theta_R)^e$	Snap-in force (μN)	Pull-off force (μN)
1	Polyurethane (PU)	70.5°	85°	48.9°	51°	36.1°	471.4 ± 14.2	179.4 ± 2.2
2	PU—2 % Silclean	98.2°	104.3°	76.3°	31°	28°	316.9 ± 17.7	175.7 ± 3.2
3	PU—8 % Silclean	104.3°	105.9°	88.1°	23°	17.8°	292.3 ± 7.3	172.6 ± 2.0
4	Polyimide	80.1°	82.5°	56.1°	26.4°	26.4°	442 ± 54.4	167.3 ± 10.3
5	Plexiglass	86.5°	93.9°	77.3°	29.1°	16.6°	387.6 ± 13.4	157.4 ± 8.1
6	Polycarbonate	92.4°	98.2°	68.1°	59.2°	30.1°	338.7 ± 22.4	163.2 ± 1.9
7	i-CVD silicone	87.9°	91.2°	62.2°	f	29°	379 ± 14.2	175.5 ± 2.6
8	i-CVD fluorosilicone	115.9°	118°	90.3°	18.2°	27.7°	141 ± 6.3	148.7 ± 1.1
9	i-CVD PTFE	127.7°	134.9°	73.6°	f	61.3°	72.4 ± 4.2	168.8 ± 1.5
10	OTS SAM	109°	117.4°	94.6°	13°	22.8°	197 ± 9.5	141.3 ± 0.2
11	FOTS SAM	107.3°	116°	95°	13.6°	21°	226.6 ± 8.7	139.5 ± 1.8
12	Perfluoroacrylate	113°	113.1°	61°	f	52.1°	398.7 ± 18.7	149.2 ± 12.6
13	Hydrophobic sol gel	112.2°	111.6°	92.4°	5.6°	19.2°	197.9 ± 12.2	111.4 ± 8.3
14	PTFE	117.7°	126.6°	91.9°	64.3°	34.7°	89.7 ± 15.4	162.0 ± 6.6
<i>Textured silicon surface (pillar diameter/spacing)</i>								
15	3/4.5 μm	149°	160°	130.8°	20°	29.2°	0	29.4 ± 2.6
16	3/6 μm	156.2°	161.3°	142.6°	10.1°	18.7°	0	15.6 ± 1.7
17	3/9 μm	154.1°	159.9°	148.9°	5.7°	11°	0	8.54 ± 0.8
18	3/12 μm	156.2°	160.8°	151.8°	3.4°	9°	0	4.71 ± 0.7
19	Rose petal—front	144.7°	150.7°	131.6°	6.1°	19.1°	2.9 ± 1.3	31.5 ± 8.0
20	Rose petal—back	132.4°	136.6°	85.7°	f	50.9°	23.4 ± 5.7	140.0 ± 15.8

^aStatic contact angle, estimated error <2°

^bAdvancing contact angle, estimated error <2°

^cReceding contact angle, estimated error <2°

^dSliding angle, estimated error <3°

^eContact angle hysteresis

^fWater droplets do not slide and are struck at 90° tilt angle

On the other hand, if one just focuses on surface **15–20** in Figs. 5.1, 5.2, and 5.3 (labeled as *open diamond*), there may exist reasonable correlations between the static contact angle and sliding angle and hysteresis. These are all superhydrophobic surfaces. The good correlations may merely indicate that if a narrow range of material property is considered, a fortuitous good correlation may be obtained.

5.2.2 Wetting and Adhesion Force Measurements

To gain a better understanding of what contact angles are measuring, Samuel, Zhao, and Law [26] measured the wetting (attractive) and adhesion force between water and surface **1–20** directly using a microbalance inside a tensiometer. A schematic of the measurement procedure is shown in Fig. 5.4, and details of the instrumentation have given elsewhere [26].

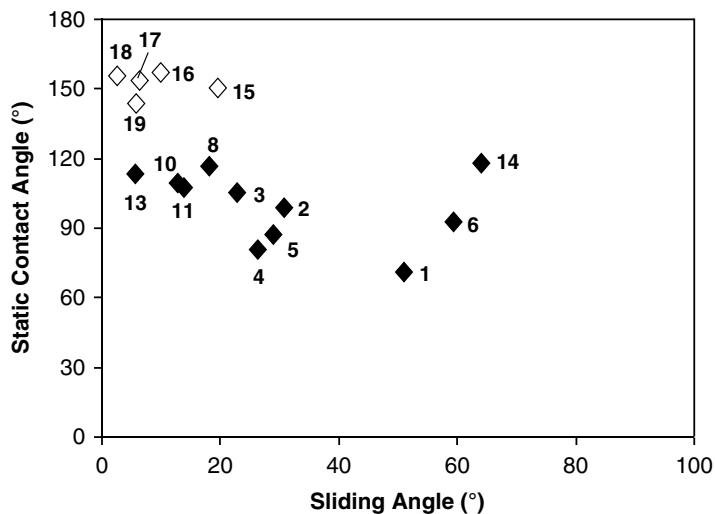


Fig. 5.1 Plots of static contact angle versus sliding angle for flat surfaces **1–14** and rough surfaces **15–19** (reproduced with permission from [26], Copyright 2011 The American Chemical Society)

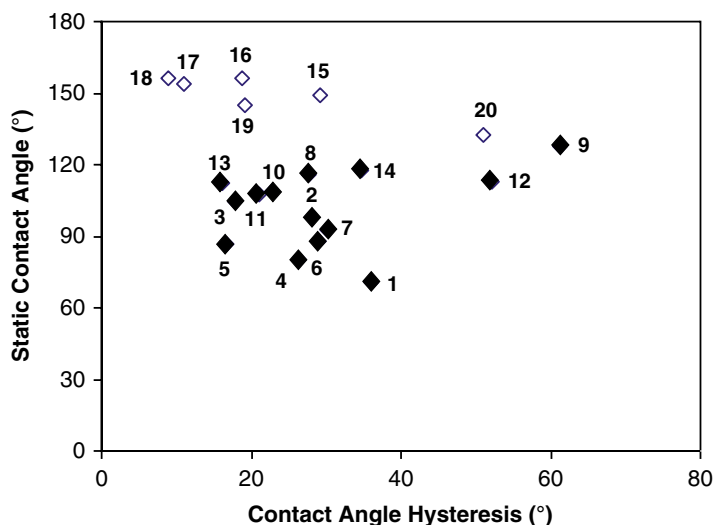


Fig. 5.2 Plots of static contact angle versus contact angle hysteresis ($\theta_A - \theta_R$) for flat surfaces **1–14** and rough surfaces **15–20** (reproduced with permission from [26], copyright 2011 The American Chemical Society)

Briefly, a 5 mg water droplet was first deposited onto a platinum ring, which is attached to a microbalance. The surface of interest is placed on a stage where it can move up and down steadily at a slow rate (10 $\mu\text{m/s}$) by a computer-controlled stepping motor. Prior to the measurement, the microbalance is set to zero. When the water drop first “touches” the surface (Fig. 5.4 step b), an attractive snap-in force

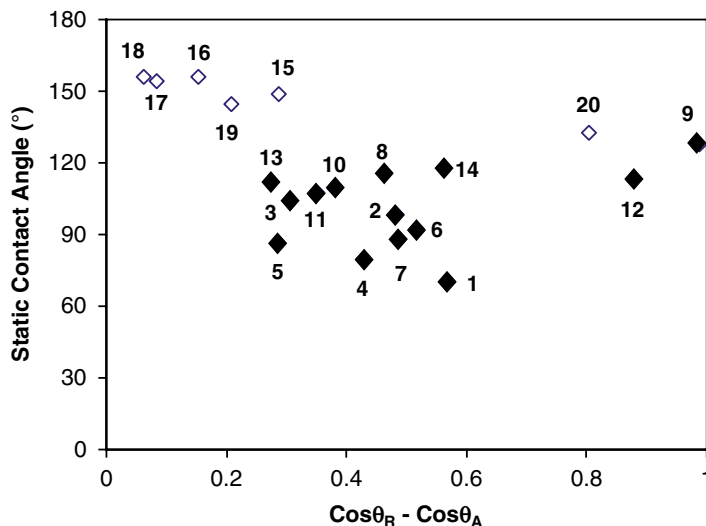


Fig. 5.3 Plots of static contact angle versus $\cos\theta_R - \cos\theta_A$ for flat surfaces 1–14 and rough surfaces 15–20 (Reproduced with permission from [26], copyright 2011 The American Chemical Society)

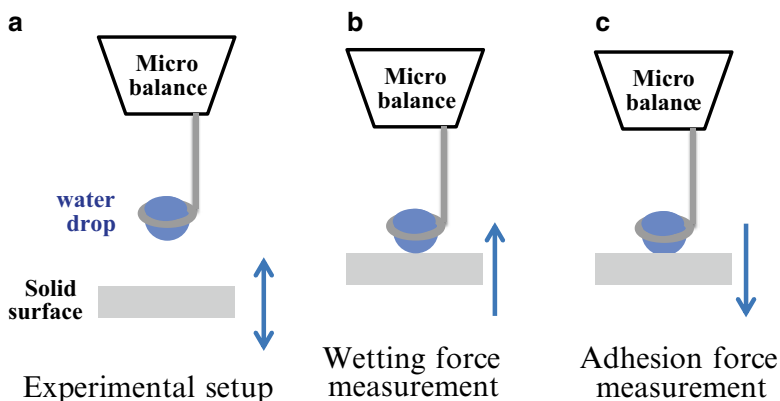


Fig. 5.4 Schematic of the apparatus and procedures for measuring the wetting and adhesion interactions between water and various surfaces. (a) Experimental setup. (b) Wetting force measurement. (c) Adhesion force measurement (reproduced with permission from [62], copyright 2014 The American Chemical Society)

attributable to the wetting interaction between the water droplet and the surface is recorded. The stronger the water–surface attraction, the stronger the snap-in force. After the water droplet and the surface made contact, the stage is retracted slowly; a pull-off force is recorded when the water droplet and the surface separate (Fig. 5.4 step c). It is worthy pointing out that the measurement of the pull-off force is a little bit more complicated. When the separation between the water droplet and the surface is clean where no residual water droplet is observed after the separation, the pull-off

force should correspond to the adhesion force between the water droplet and the surface at vertical separation. However, when a residual water droplet is observed on the surface after the pull-off, it implies that the adhesion between the surface and the water droplet is stronger than the cohesive force within the water droplet. What's recorded is the force when the water droplet breaks. The magnitude of this force is related to the adhesion between the water droplet and the surface, cohesive force of the water droplet (surface tension), and the contact area when the water droplet breaks. This is actually a very important observation. The implication of the residual droplet to surface definition will be discussed further in the next chapter in this book. Here, we assume that the measured force is still dominated by the adhesion force between the water droplet and the surface. Both snap-in force and pull-off force data for the water droplet on surfaces 1–20 are included in Table 5.1.

5.2.3 Wetting Interaction and Contact Angles

Numerous attempts were made to correlate the contact angle data from surfaces 1–20 with the force data. The snap-in force, which measures how strongly the water droplet and the surface interact, is shown to correlate well with θ_A . Figure 5.5 plots the snap-in force on surfaces 1–20 versus θ_A . The snap-in force increases monotonously

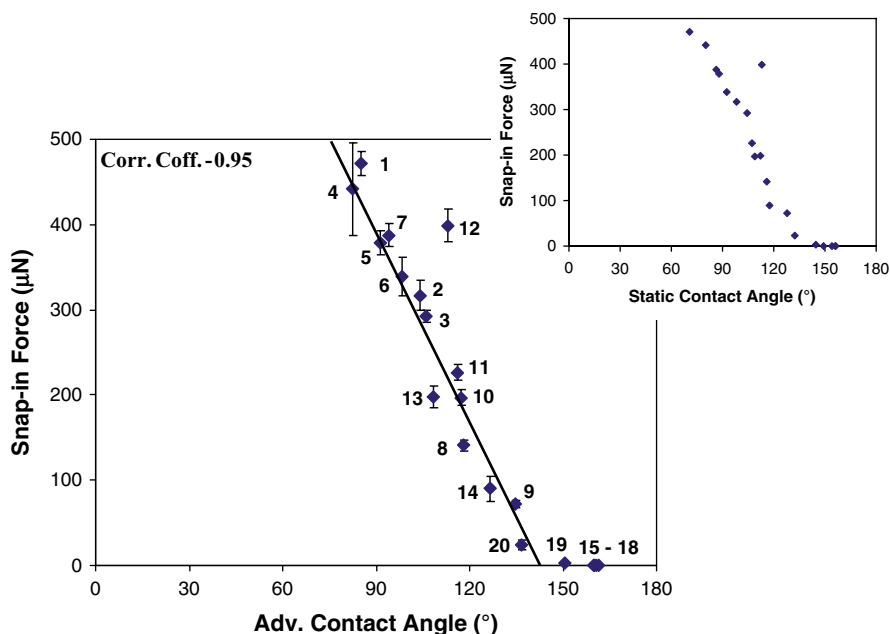


Fig. 5.5 Plot of snap-in force versus advancing contact angle (*inset*: plot of snap-in force versus static contact angle) (reproduced with permission from [26], copyright 2011 The American Chemical Society)

as θ_A decreases. Since snap-in force measures the strength of the water attraction, the correlation indicates that θ_A correlates to surface wettability; the larger the θ_A value, the lower the surface wettability. The snap-in force becomes negligible at $\theta_A \geq 145^\circ$, indicating that there is practically no attractive interaction between water and surfaces **15–19**. The significance of this observation will be discussed in Chap. 6. Incidentally, a reasonably good correlation is also obtained when the snap-in force is plotted against θ (inset of Fig. 5.5). The observation is not unexpected since static contact angle θ always tracks well with the advancing contact angle θ_A due to the way the two measurements are made.

5.2.4 Adhesion Interaction and Contact Angles

Sliding angle α is the tilt angle when the sessile droplet starts to move on an inclined surface. It measures stickiness of the surface or mobility of the liquid droplet; the stickier the surface, the larger the sliding angle and the lower the drop mobility. As a result, a number of reports suggested that α , contact angle hysteresis ($\theta_A - \theta_R$), and $(\cos\theta_R - \cos\theta_A)$ are related to surface adhesion [11, 27–30]. Since the pull-off force measures the adhesion between the water droplet and the surface, we can then test these hypotheses by plotting the pull-off force against α , ($\theta_A - \theta_R$), and $(\cos\theta_R - \cos\theta_A)$. The results are shown in Figs. 5.6, 5.7, and 5.8, respectively. In these plots, the surfaces are further classified into two groups. Specifically, surfaces labeled with *open squares* are surfaces that are clean after pull-off (no residual water droplet), and *solid squares* are surfaces with a small residual water droplet left behind after

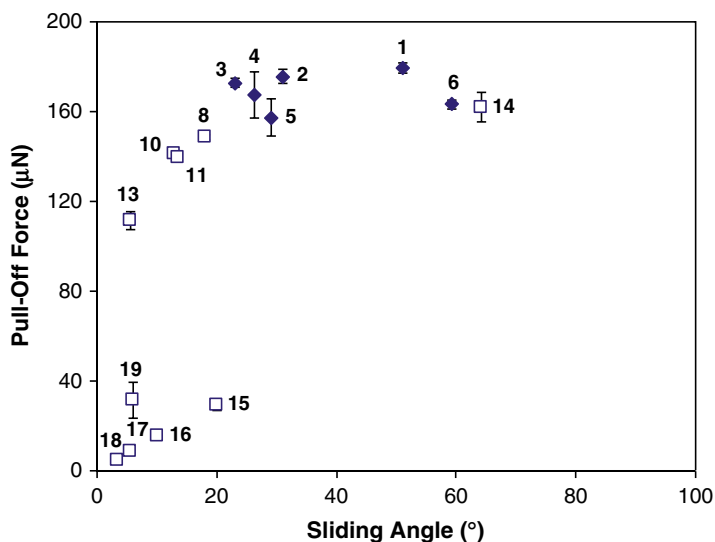


Fig. 5.6 Plot of the pull-off force for surfaces **1–20** versus sliding angle α (reproduced with permission from [26], copyright 2011 The American Chemical Society)

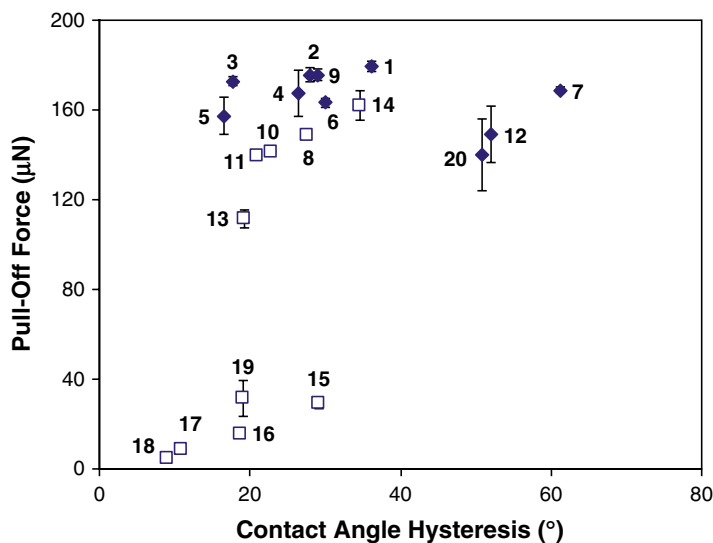


Fig. 5.7 Plot of the pull-off force for surfaces **1–20** versus contact angle hysteresis ($\theta_A - \theta_R$) (reproduced with permission from [26], copyright 2011 The American Chemical Society)

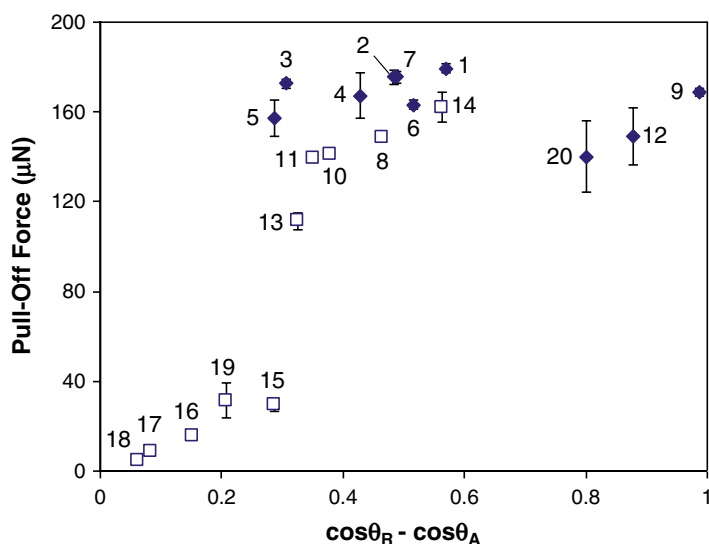


Fig. 5.8 Plot of the pull-off force for surfaces **1–20** versus $\cos\theta_R - \cos\theta_A$. (Reproduced with permission from [26], copyright 2011 The American Chemical Society)

pull-off. Examination of the data suggests that there is little correlation between the pull-off force on surfaces **1–20** with the sliding angle α , contact angle hysteresis ($\theta_A - \theta_R$), and $(\cos\theta_R - \cos\theta_A)$. The absence of any correlation implies that α , $(\theta_A - \theta_R)$, and $(\cos\theta_R - \cos\theta_A)$ are not measures of surface adhesion. On the other hand, further

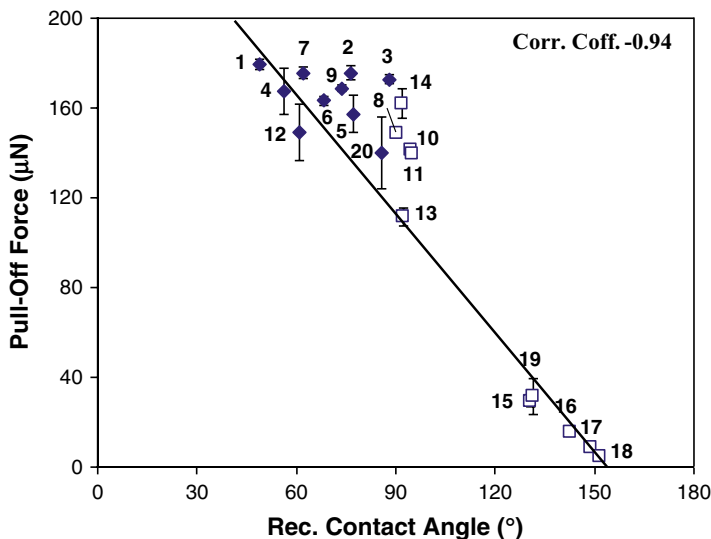


Fig. 5.9 Plot of the pull-off force versus receding contact angle from surfaces 1–20 (reproduced with permission from [26], copyright 2011 The American Chemical Society)

examination of the data reveals that some correlation may exist if one groups the surfaces into two different sets. The first set of surfaces includes 1–14 and 20. Similar to the combined set of data, this group of surfaces shows no correlation with sliding angle α , contact angle hysteresis ($\theta_A - \theta_R$), and $(\cos\theta_R - \cos\theta_A)$. The second set of surfaces, 15–19, are all superhydrophobic. The water droplet is in the Cassie–Baxter state on these surfaces. The pull-off force seems to correlate well to the sliding angle α , contact angle hysteresis ($\theta_A - \theta_R$), and $(\cos\theta_R - \cos\theta_A)$. The characteristic of this set of surfaces is that water pulls off cleanly from these surfaces and they all have a relatively low pull-off force. Of course, one can always argue that this correlation only occurs over a narrow range of contact angles. Or this correlation only happens with rough surfaces.

On the other hand, when the pull-off force is plotted against the receding contact angle of surfaces 1–20, a good correlation is obtained (Fig. 5.9). Pull-off force increases monotonically as the receding angle decreases. The data appears to be more scattered at smaller receding contact angles, presumably due to the involvement of different “separating states” in the pull-off measurements. The water drop may break differently depending on specificity of the interaction. In any event, the result in Fig. 5.9 suggests that receding contact angle correlates well to surface adhesion. Another significant observation in Fig. 5.9 is that there appears to be a cutoff at receding angle 90° where surfaces are clean and without any residual water droplet after pull-off when θ_R is $>90^\circ$. This point will be discussed further in Chap. 6.

The work of adhesion (W_h) between a liquid droplet and the surface can be quantified as shown in (5.1) according to the surface literature [24, 30].

$$W_h = \gamma_{LV} (1 + \cos\theta_R) \quad (5.1)$$

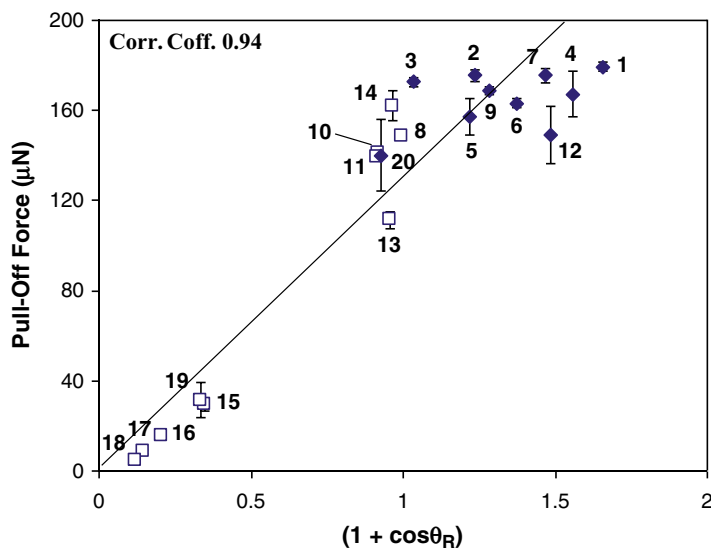


Fig. 5.10 Plot of pull-off force measured on the tensiometer versus $(1 + \cos\theta_R)$ (reproduced with permission from [26], copyright 2011 The American Chemical Society)

Thus, if the pull-off force is a measure of surface adhesion, it should correlate to $(1 + \cos\theta_R)$. Indeed, a good linear correlation is obtained in Fig. 5.10 when the pull force is plotted against $(1 + \cos\theta_R)$. The overall result confirms that the pull-off force indeed measures the adhesion between the water droplet and the surface when they separate during the experiment in the tensiometer. More importantly, the plot in Fig. 5.10 establishes convincingly that receding angle θ_R indeed measures adhesion. The fundamental reason why θ_R is correlating to surface adhesion is because θ_R is dictated by the ability of the liquid droplet to de-pin at the liquid–solid interface; the smaller the θ_R , the more difficult it is to de-pin and the stronger the adhesion interaction.

5.3 Sliding Angle

When the sessile droplet on a horizontal surface is tilted, the normally circular droplet is distorted or elongated by gravity. The degree of distortion is related to the contact angle hysteresis and the angle of tilting [27, 28]. Figure 5.11a depicts a schematic of a distorted sessile droplet on an inclined surface and the forces that act on the liquid droplet on the tilted surface. The driving force (F) for a liquid droplet to slide is gravity and is given by

$$F = mg \cdot \sin \alpha \quad (5.2)$$

where m is the mass of the liquid droplet and g is the gravitational constant.

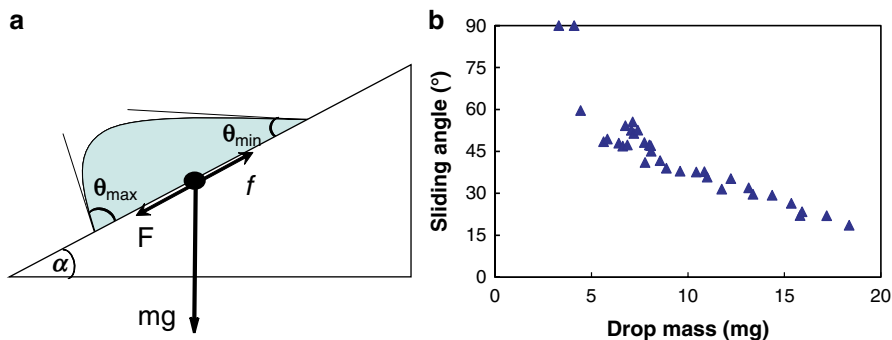


Fig. 5.11 (a) Schematic of a distorted sessile drop on a tilted surface and (b) plot of sliding angle as a function of drop mass for hot polyethylene wax droplets on FOTS-treated silicon wafer

Sliding angle α is the tilt angle moment before drop sliding. Thus, α is a measure of surface stickiness or drop mobility. For a given drop mass, surface stickiness increases as α increases. Figure 5.11b shows a typical decrease profile for the sliding angle as a function of drop mass. It is therefore important to control and know the drop mass (or volume) when comparing surface stickiness or drop mobility from sliding angle data.

The retention (or frictional) force (f) that keeps the drop from sliding is a lot more difficult to determine. The schematic in Fig. 5.11a is just a simplified view of the situation. In short, the sessile droplet is distorted three dimensionally. Figure 5.12a shows a photograph of a water drop on a tilted surface. The smallest angle of contact for the distorted drop is at the trail edge and is designed as θ_{\min} . The angle of contact increases along the contact line downward; the largest angle is observed at the lead edge and is designated as θ_{\max} [31]. A 2D top view showing the change in the angle of contact around the three-phase contact line of the distorted droplet is given in Fig. 5.12b. Principally, the retention force is the sum of all forces around the circumference of the distorted droplet [32]. To make the problem manageable, Furmidge [29] and Macdougall and Ockrent [30] simplified the complex 3D geometry to 2D, and f can be expressed as

$$f = \gamma_{LV} \cdot R \cdot k \cdot (\cos \theta_{\min} - \cos \theta_{\max}) \quad (5.3)$$

where γ_{LV} is the surface tension of the liquid, R is the length scale for the contour of the drop, and k is an adjustable parameter based on experimental data.

Just before drop sliding on the tilted surface, $F=f$. Krasovitski and Marmur [33] equated the sliding angle to θ_{\max} and θ_{\min} as

$$\sin \alpha = C \cdot \gamma_{LV} \cdot (\cos \theta_{\min} - \cos \theta_{\max}) \quad (5.4)$$

where C is a constant that includes the gravitational acceleration, density of the liquid, and the geometric parameters of the drop.

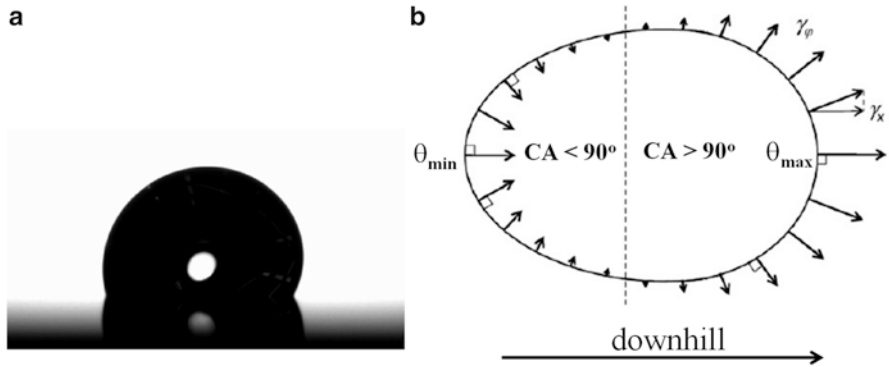


Fig. 5.12 (a) A photograph of a water droplet on a tilted surface and (b) schematic showing the forces acting on the sessile drop on the tilted surface (b, reproduced with permission from [32], copyright 2008 Elsevier)

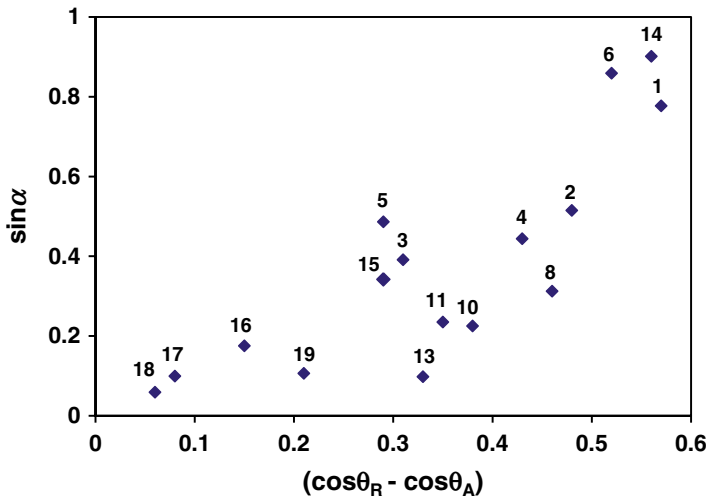


Fig. 5.13 Plot of $\sin \alpha$ for surfaces in Table 5.1 versus $(\cos \theta_R - \cos \theta_A)$

In the surface science literature, it was shown as early as 1942 that the lead edge and trail edge angles on the tilted plane are θ_A and θ_R , respectively [30]. More recently, ElSherbini and Jacobi [34] reported that θ_{min} and θ_{max} are approximately equal to θ_R and θ_A for a large number of liquid–surface combinations. If that is true, plot of $\sin \alpha$ versus $(\cos \theta_R - \cos \theta_A)$ (data in Table 5.1) should yield a linear relationship. Experimentally, a very scattered plot is obtained in Fig. 5.13. Although there is a very rough trend, the lack of a good linear correlation suggests that $\theta_{max} \neq \theta_A$ and $\theta_{min} \neq \theta_R$. This is not a surprising outcome because many approximations have been used to derive at Eq. (5.4). After all, both Pierce et al. [32] and Krasovitski and

Marmur [33] demonstrated that there is only a limited contact angle hysteresis range that $\theta_{\max}=\theta_A$ and $\theta_{\min}=\theta_R$. The general assumption that the lead edge and trail edge angle of a tilted liquid drop are θ_A and θ_R is highly questionable. Therefore, we would not recommend using the titling plane method to determine θ_A and θ_R .

5.4 Contact Angle Hysteresis

5.4.1 What Does It Measure?

Contact angle hysteresis defines as the difference between θ_A and θ_R . Results in Figs. 5.2 and 5.7 show that it does not correlate to the static contact angle θ and receding angle θ_R . This indicates that contact angle hysteresis is neither measuring surface wettability nor adhesion directly. Similar conclusion was also reached by Della Volpe et al. [35], who concluded that contact angle hysteresis is completely independent of the hydrophobicity/hydrophilicity of the surface. On the other hand, many researchers have suggested that low hysteresis is the main reason for high drop mobility on tilted surfaces [36–39]. Since sliding angle α is a direct measure for drop mobility, a plot of sliding angle α versus (θ_A and θ_R) from the data in Table 5.1 should be a good test for the hypothesis. Experimentally, a scattered plot (Fig. 5.14) is obtained. The scattered plot suggests that if hysteresis is correlating to drop mobility, the correlation is only qualitative at best. Indeed, Pierce, Carmona, and Amirfazli [32] also concluded that advancing and receding contact angles are not good predictors for drop mobility in their detailed analysis of the complicated

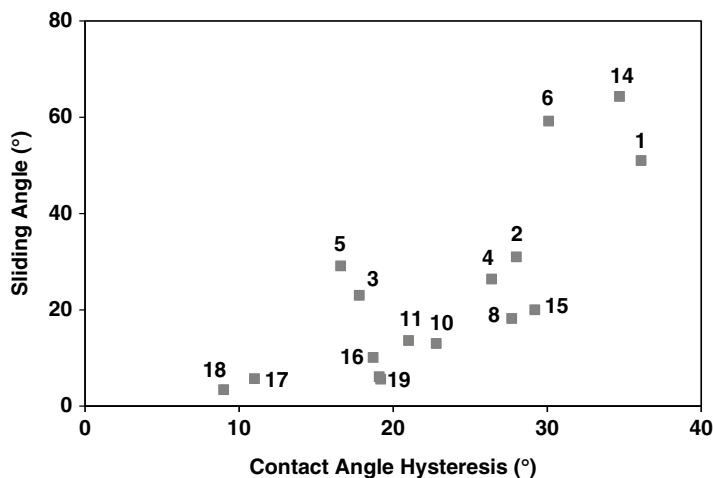


Fig. 5.14 Plot of sliding angle α for surfaces in Table 5.1 versus contact angle hysteresis

relationship among sliding angle, advancing and receding contact angle, and hysteresis.

As pointed out earlier in Chap. 3, both θ_A and θ_R are angles from their respective metastable wetting states. Their equivalent Young's equations can be written as

$$\cos \theta_A = \frac{\gamma_{SV} - \gamma_{SL}^{ad}}{\gamma_{LV}} \quad (5.5)$$

$$\cos \theta_R = \frac{\gamma_{SV} - \gamma_{SL}^{re}}{\gamma_{LV}} \quad (5.6)$$

where γ_{SV} and γ_{LV} are the surface tensions for the solid and liquid, respectively, γ_{SL}^{ad} is the liquid–solid interfacial tension during advancing, and γ_{SL}^{re} is the liquid–solid interfacial tension during receding.

During receding, the area underneath the drop is already wetted. The contact line is receding from an interface where liquid molecules and solid–surface materials are already relaxed and are in their equilibrated state. This may not be the case during advancing. Liquid molecules and materials on the solid surface may not have enough time to equilibrate at the interface as the contact line is kept advancing. In other words, there is a difference in liquid–solid interfacial tension in the advancing mode and the receding mode (γ_{SL}^{ad} versus γ_{SL}^{re}). Therefore, contact angle hysteresis is actually a measure of the difference in liquid–solid interfacial tension during advancing and during receding; the larger the difference, the larger the hysteresis.

5.4.2 Mechanisms for Contact Angle Hysteresis

Equations (5.5) and (5.6) clearly show that contact angle hysteresis originates from the difference in liquid–solid interfacial tension during advancing and during receding. The difference in wetting states during advancing and receding was mentioned by Macdougall and Ockrent [30] and by Pease [40] earlier. Historically, contact angle hysteresis was attributed to roughness and heterogeneity [7, 9, 41, 42]. Indeed, when a liquid is in the Wenzel state, it wets the rough surface fully and results in pinning of the liquid droplet on the surface and very large hysteresis [43, 44]. Extrand [45] further suggested that the geometry of the roughness may be more important than roughness alone in determining the contact angle and hysteresis of ultraphobic pillar array surfaces. It thus appears that roughness is not the only contributor to contact angle hysteresis.

The occurrence of sizable contact angle hysteresis on perfectly smooth surfaces was reported as early as 1952 by Bartell and Bjorklund [46] in a three-liquid, three-phase system comprising mercury, benzene, and water. A strong conclusion was not drawn that time presumably due to the observation of an unexplained, aging phenomenon on the three-liquid system. Four decades later, Chen and coworkers [47] reported a study of the contact angle hysteresis of several monolayer modified mica

sheets with water and observed sizable hysteresis also despite working with atomic smooth samples. They attributed the large hysteresis to the relaxation of liquid molecules after the liquid wets the monolayer–mica surfaces. Rearrangement of functional groups in polymer chains and dipoles in liquid after wetting was reported at the water–hydrogel interfaces, which lead to large hysteresis [48]. Lee and coworkers demonstrated the existence of interactions between liquid molecules and dipoles on different fluoropolymer surfaces during their wettability study [49]. Extrand and Kumagai [50] designed an experiment consisting of six different surfaces (silicon wafer plus five different polymers) and five different liquids, to test whether roughness or chemical interaction at the interface are playing a role in determining the contact angle hysteresis. The 6×5 matrix includes liquid–surface combinations with a wide range of contact angle and hysteresis. They concluded that chemical interaction at the liquid–solid interface is a key contributor to the large hysteresis observed in their study. It thus becomes apparent that both chemical and physical interactions can contribute to contact angle hysteresis. Before the liquid wets the solid surface, molecules in liquid droplet and on the surface of the solid are in their respective thermodynamically stable state. As soon as the liquid wets the surface, both liquid molecules and segments of materials on the solid surface can rearrange to their relaxed state at the liquid–solid interface. The degree of relaxation will depend on the specific liquid–solid system. Surface roughness can magnify the interaction. Using the methodology of Cassie–Baxter, the total contact angle hysteresis (CAH^{tot}) for a given liquid–solid system can be defined as

$$\text{CAH}^{\text{tot}} = f_s \cdot \text{CAH}^{\text{chem}} + (1 - f_s) \cdot \text{CAH}^{\text{rough}} \quad (5.7)$$

where f_s is the solid area fraction on the rough surface, CAH^{chem} is the CAH from the chemical interaction, and $\text{CAH}^{\text{rough}}$ is the CAH from the rough structure.

For smooth surfaces, $f_s = 1$, the chemical interaction between molecules in the liquid and the solid surface (CAH^{chem}) becomes the sole contributor. For rough surfaces, both CAH^{chem} and $\text{CAH}^{\text{rough}}$ are contributing to the hysteresis observed. Generally speaking, CAH^{tot} for rough surface increases as f_s increases due to the pinning effect [51, 52]. For surfaces similar to the Lotus leaf, f_s approaches zero and $\text{CAH}^{\text{rough}}$ dictates the size of the hysteresis. Factors that govern $\text{CAH}^{\text{rough}}$ have not been well studied. Many investigators have been using measured roughness factors, such as Ra and Rz, to correlate contact angle data and usually not very fruitful. In any event, if one considers the interaction between the liquid and the rough structure at the molecular level, one would intuitively expect that the pinning geometry at the three-phase contact line should be paramountly important. Indeed, Extrand found in his study of the wetting of pillar array surfaces that the decrease of receding contact angle and increase of hysteresis is more sensitive to the geometry of the pillar than the height [45]. Very recently, Kanungo and coworkers reported that the hystereses of PDMS surfaces with bumps are larger than those with cavities for the same roughness factor in their study of the wetting of water on rough PDMS surfaces [53]. To an extreme, rough surfaces with vertical protrusion, even in the nanoscale,

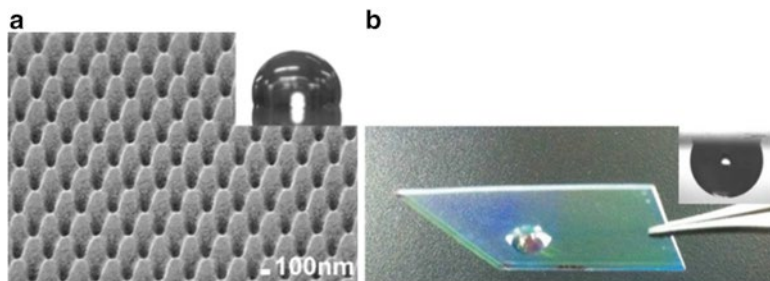


Fig. 5.15 (a) SEM micrograph of a polycarbonate film with nanosized protrusion (pitch and height are ~ 300 nm) and (b) polycarbonate film flipped 180° (insets: images of the sessile droplets) (reproduced with permission from [54], copyright 2014 The American Chemical Society)

are found to be very effective in immobilizing liquid droplets due to pinning. This of course results in a very large contact angle hysteresis. For instance, Law et al. [54] recently prepared a series of polycarbonate films with nanosized protrusion by the nanoimprinting technique and found that water droplet basically pins on the rough surface during wetting. Figure 5.15a shows a SEM micrograph of a nano-patterned polycarbonate surface (pitch and height are ~ 300 nm) and the water sessile droplet image. The water contact angle was at 108° . The contact angle is larger than that of a smooth polycarbonate surface ($\sim 92^\circ$), indicating that water is in the Wenzel state on the nano-patterned surface. Indeed, water droplet was found stuck and pinned when the surface is flipped 180° (Fig. 5.15b). The nano-patterned surface is thought to be useful in preventing the so-called coffee ring stain effect during inkjet printing. Similarly, Mettu, Kanungo, and Law [55] also observed analogous pinning effect on a biaxial-oriented polypropylene (BOPP) substrate. Nanosized vertical protrusions were shown to form upon heating, and the resulting protrusions pin droplets of the inkjet materials on the heated BOPP surface.

5.5 Surface Characterization Recommendations

Contact angle measurement has been a very popular tool to characterize the property of solid surfaces and understand liquid–solid interactions. Based on the data summarized in this chapter (Figs. 5.1, 5.2, 5.3, 5.4, 5.5, 5.6, 5.7, 5.8, 5.9, 5.10, 5.11, 5.12, 5.13, and 5.14), we recommend that surface should be characterized by its advancing contact angle, receding contact angle, and sliding angle. They measure surface wettability, adhesion, and stickiness or slipperiness, respectively (Fig. 5.16). In theory, static contact angle is not a measure of anything. However, researchers often found θ to correlate to the advancing angle and wettability (e.g., Fig. 5.5). This is probably due to the way both measurements are made. Specifically, both static and advancing angles involve contact line advancing prior to capturing and analyzing of

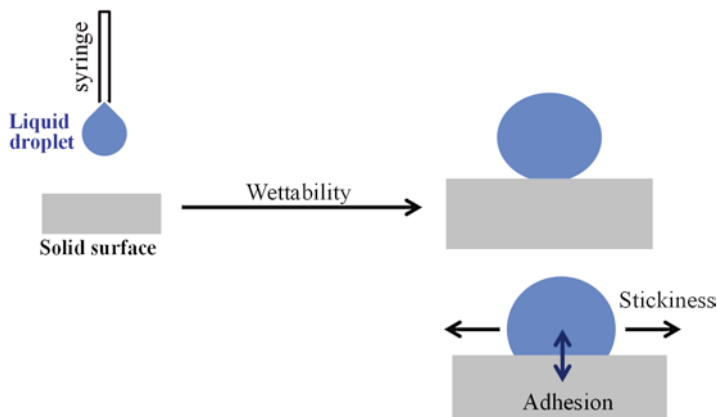


Fig. 5.16 A summary of surface characterization recommendations

the drop profile. From the liquid–solid interaction perspective, advancing contact angle will give indication if a liquid will wet or repel by a surface. Receding contact angle will allow prediction of the strength of the liquid–solid adhesion, while sliding angle will offer clue about mobility of the liquid droplet.

As discussed previously, contact angle hysteresis has been said to correlate to adhesion and drop mobility in the literature. We have to emphasize that, from the data in Figs. 5.7 and 5.14, the correlation is qualitative at best. The main reason for the existence of a rough correlation is because of the θ_R term in contact angle hysteresis. While it may be a surprise to some, hysteresis is not related to wettability either [35]. Undoubtedly more work is needed to understand the true role of contact angle hysteresis in surface characterization and wetting, Eqs. (5.5) and (5.6) clearly indicate that it originates from the difference in liquid–solid interfacial tension during advancing and during receding. In other words, the liquid–solid interface can be in two different states depending on whether it is in the advancing or receding mode. It is only with this understanding that we can comprehend some of the unexpected results reported in recent surface literature, e.g., surfaces with both small contact angle and sliding angle. These surfaces will be part of the conversation in the next section.

5.6 Myths in Adhesion and Contact Angle Hysteresis

There are many myths in surface science. One of them is the belief that large contact angle would lead to low adhesion, low hysteresis, and nonstickiness. The report of the self-cleaning effect displayed by the Lotus leaf further exacerbates that belief [56]. In any event, the self-cleaning effect did inject excitement in surface science and engineering. Studies of superhydrophobicity and more recently superoleophobicity have been fierce and intense. Numerous potential applications, e.g., self-cleaning textiles; oil- and soil-resistant clothing; anti-smudge surface for iPhone

Table 5.2 Contact angle data highlighting the expected and unexpected surface properties reported in recent literature

Surface	Liquid	θ^a	α^b	θ_A^c	θ_R^d	$\theta_A - \theta_R^e$	References
i. Lotus leaf	Water	162°	4°				[56]
ii. FOTS-coated textured Si wafer (~3 $\mu\text{m}/12 \mu\text{m}/\sim 7 \mu\text{m}/\text{wavy}$) ^f	Water	156°	3.4°	161°	152°	9°	[51]
	Hexadecane	154°	3.7°	162°	142°	20°	
iii. FOTS-coated textured Si wafer (~3 $\mu\text{m}/6 \mu\text{m}/\sim 7 \mu\text{m}/\text{smooth}$) ^f	Water	152°	12°	162°	135°	27°	[57]
	Hexadecane	120°	Not slide	129°	~0°	~129°	
iv. Hydrophobized SU8 texture on Si wafer (20 $\mu\text{m}/32 \mu\text{m}/30 \mu\text{m}$) ^g	Water	–	Not slide	140°	~0°	~140°	[44]
v. OTS SAM on Si wafer ^a	Water	109°	13°	117°	95°	22°	[57]
	Hexadecane	40°	8°	45°	34°	10°	
vi. FOTS SAM on Si wafer ^b	Water	107°	13°	116°	95°	21°	[57]
	Hexadecane	73°	9°	75°	65°	10°	
vii. PDMS ^{2K} on glass ^h	Water	–	–	104°	102°	2°	[58]
viii. PDMS ^{9K} on glass ^h	Water	–	–	106°	105°	1°	[58]
ix. PU—Fluorolink	Hexadecane	68°	7°	–	–	–	[59]
x. C10 sol gel hybrid film	Hexadecane	–	3.4°	36°	34°	2°	[60]
xi. PU—2 % SiClean	Water	90°	31°	104°	76°	28°	[57]
	Hexadecane	31°	6°	–	–	–	
xii. PU—8 % SiClean	Water	104°	23°	106°	88°	18°	[57]
	Hexadecane	34°	2°	–	–	–	

^aStatic contact angle, estimated error <2

^bSliding angle, estimated error <3

^cAdvancing contact angle, estimated error <2

^dReceding contact angle, estimated error <2

^eContact angle hysteresis

^fPillar diameter/pitch/height/sidewall

^gSquare pillar/pitch/height

^h2K and 9K denote the molecular weight of the PDMS chains

and display; anti-icing coating for power lines, rooftops, and airplanes; corrosion-resistant coating for bridges and other metal structures; drag reduction in ship; gas and fuel transportation; microfluidic devices; etc., are being pursued worldwide. Many interesting surface properties have been reported. Some of the counterintuitive observations include (1) large contact angle surfaces with large sliding angles and hysteresis and (2) small contact angle surfaces with low hysteresis and high drop mobility. While the literature data is massive, in Table 5.2 we highlight some of the key examples to illustrate the usefulness of a better understanding of basic concepts in comprehending these unexpected results.

Surfaces i–iv are rough surfaces whose surface properties and structures are well characterized. While Lotus leaf i [56], artificial superhydrophobic surfaces ii and iii (with water), and superoleophobic surfaces ii (with hexadecane) [51, 57] all exhibit the expected large contact angle with small sliding angle and low hysteresis, sticky rough surfaces with large contact angles in the cases of iii (hexadecane) and iv

(water) are less common [44, 57]. The probing liquids in both cases fully wet the rough surfaces and are in the Wenzel state [43]. According to the Wenzel equation, the static contact angle should decrease if the surface material is hydrophilic or oleophilic, but the contrary is observed in the cases of iii (hexadecane) and iv (water). The observation is in violation with the Wenzel equation and is attributable to the pinning effect. Detail discussion of the pinning effect and the mechanism for producing the unexpected large contact angle has been given in Sect. 4.2.2 in this book.

Surfaces v–xii are smooth flat surfaces and they are all hydrophobic (water $\theta > 90^\circ$). Their contact angles, sliding angles, and hysteresis are not correlated to common intuition, e.g., the water advancing contact angles θ for v and vi are larger than those of vii and viii, but their sliding angles and hysteresis are larger too! The results are consistent with the scattered plots shown in Figs. 5.1, 5.2, and 5.3. Counterintuitive results are also observed when hexadecane is used as the probing liquid. Surfaces v, vi, and ix–xii all exhibit low contact angles: θ , θ_A , and θ_R . While the low contact angles are expected due to the low surface tension of hexadecane (27.5 mN/m as compared to 72.8 mN/m for water), what's unexpected are their low ($< 10^\circ$) sliding angles and small hysteresis. These results imply that these surfaces are highly wettable with high adhesion. On the other hand, the small sliding angles suggest that these surfaces are actually nonsticky. How can that be? The high adhesion and nonsticky properties seem to contradict to each other. However, the observations can be rationalized based on the thermodynamic of the wetting and de-wetting process. Specifically, when $\theta_A \approx \theta_R$, the energy that is required to de-pin the drop is likely well compensated by the energy gained from the favorable wetting process. Using several low-hysteresis examples, McCarthy et al. [38, 58] conjectured earlier that kinetic factor, namely, low activation barrier for the de-pinning process, is the main reason for the high drop mobility. We feel that while low activation energy barrier to de-pin the receding contact line may be the effect, the real cause for the high mobility is still the favorable thermodynamic of the wetting/de-wetting process. These low-hysteresis surfaces may find applications as anti-graffiti coating and easy-clean, self-clean surfaces for inkjet printheads [59, 61].

The unusual surface property exhibited by v–xii may offer new avenue for the designs of new self-cleaning surfaces of varying contact angles. It may shine new lights into the mechanism of contact angle hysteresis. For example, surfaces vii–xii all comprise low-surface-energy functional groups at the surfaces, e.g., the C10 hydrocarbon chain, oligomers of polydimethylsiloxane, and the perfluoropolyether polymer chain. These low-surface-energy functional groups are all known to be flexible, and they will migrate outward toward the air–surface interface during coating and drying. Incidentally, these low-surface-energy functional groups are also compatible with hexadecane. The favorable hexadecane–surface interactions have resulted in high wettability and low θ_A for surfaces ix–xii. During receding, the contact line recedes from the wetted area where equilibration at the interface between liquid molecules and the solid surfaces has already occurred. The receding angle is dictated by interfacial tension γ_{SL}^{re} . We further suggest that due to the compatibility between hexadecane and these low-surface-energy, flexible functional groups, materials at the liquid–solid interface also get their chance to equilibrate

during advancing. As a result, the liquid–solid interfacial tension during advance, $\gamma_{\text{SL}}^{\text{ad}}$, is very similar to $\gamma_{\text{SL}}^{\text{re}}$. Consequently, θ_{A} is similar to θ_{R} according to Eqs. (5.5) and (5.6) and very low hysteresis is resulted. Additional evidence to support this concept comes from the contact angle data in surfaces v and vi. Comparison of the water and hexadecane contact angle data reveal that probing the surfaces with water always leads to larger contact angles, θ , θ_{A} , θ_{R} , and α as well as larger hysteresis as compared to those of hexadecane. There appears an inverted correlation between favorability of the liquid–solid interaction and contact angle. For example, with stronger interfacial interactions between hexadecane and the C18 hydrocarbon chain and the C8 perfluorocarbon chain in the monolayers of the OTS SAM and FOTS SAM, the contact angles, sliding angles, and hysteresis with hexadecane are found to be all smaller than those with water.

References

1. Young T (1805) An essay on the cohesion of fluids. *Philos Trans R Soc Lond* 95:65–87
2. Rayleigh L (1890) On the tension of water surfaces, clean and contaminated, investigated by the method of ripples. *Philos Mag* 30:386–400
3. Bartell FE, Wooley AD (1933) Solid–liquid–air contact angles and their dependence upon the surface condition of the solid. *J Am Chem Soc* 55:3518–3527
4. Bartell FE, Hatch GB (1934) Wetting characteristics of Galena. *J Phys Chem* 39:11–24
5. Dupre A (1869) *Theorie Mechanique de la Chaleur*. Gauthier-Villars, Paris, p 369
6. Gibbs JW (1928) *Trans. Connecticut Acad.* 1876–1878, 3; *Collected Works*, vol. 1. Longmans, Green, New York
7. Shuttleworth R, Bailey GJ (1948) The spreading of a liquid over a rough surface. *Discuss Faraday Soc* 3:16–22
8. Morra M, Occhiello E, Garbassi F (1990) Knowledge about polymer surfaces from contact angle measurements. *Adv Colloid Interface Sci* 32:79–116
9. Joanny JF, de Gennes PG (1984) A model for contact angle hysteresis. *J Chem Phys* 81:552–561
10. Good RJ (1977) Surface free energy of solids and liquids: thermodynamics, molecular forces, and structures. *J Colloid Interface Sci* 59:398–418
11. Carre A, Shanahan MER (1995) Drop motion on an inclined plane and evaluation of hydrophobic treatment on glass. *J Adhes* 49:177–185
12. Bormashenko E, Bormashenko Y, Oleg G (2010) On the nature of the friction between nonstick droplets and solid substrates. *Langmuir* 26:12479–12482
13. Xiu Y, Zhu L, Hess DW, Wong CP (2008) Relationship between work of adhesion and contact angle hysteresis on superhydrophobic surfaces. *J Phys Chem C* 112:11403–11407
14. Lv C, Yang C, Hao P, Feng H, Zheng Q (2010) Sliding of water droplet on microstructured hydrophobic surfaces. *Langmuir* 26:8704–8708
15. Ko YC, Ratner BD, Hoffman AS (1981) Characterization of hydrophilic–hydrophobic polymer surfaces by contact angle measurements. *J Colloid Interface Sci* 82:25–37
16. Morra M, Occhiello E, Garbassi F (1989) Contact angle hysteresis on oxygen plasma treated polypropylene surfaces. *J Colloid Interface Sci* 132:504–508
17. Tsibouklis J, Nevell TG (2003) Ultra-low surface energy polymers. The molecular design requirements. *Adv Mater* 15:647–650
18. Strohmeier BR (1993) Improving the wettability of aluminum foil with oxygen plasma treatment. In: Mittal KL (ed) *Contact angle, wettability and adhesion*. VSP BV, Zutphen, pp 453–468

19. Tsai YC, Chou CT, Penn LS (1993) Contact angle data and adhesive performance for smooth surfaces with attached molecular chains. In: Mittal KL (ed) Contact angle, wettability and adhesion. VSP BV, Zutphen, pp 729–737
20. Murase H, Fujibayashi T (1997) Characterization of molecular interfaces in hydrophobic systems. *Prog Org Coat* 31:97–104
21. Rios PF, Dodiul H, Kenig S, McCarthy S, Dotan A (2007) The effect of polymer surface on the wetting and adhesion of liquid systems. *J Adhes Sci Technol* 3–4:227–241
22. Jao SHE, Chen JH, Shifley JD, Aslam M, Pavlisko JA (2009) Electrophotographic apparatus. US Patent 7,565,091
23. Hasebe S (2008) Numerical simulation of the toner melting behavior in fuser nip considering toner rheology. NIP24 and Digital Fabrication 2008. Final Program and Proceedings, Pittsburgh, pp 519–522
24. Gao L, McCarthy TJ (2008) Teflon is hydrophilic. Comments on definitions of hydrophobic, shear versus tensile hydrophobicity and wetting characterization. *Langmuir* 24:9183–9188
25. Mittal KL (ed) (1993) Contact angle, wettability and adhesion. VSP BV, Zutphen
26. Samuel B, Zhao H, Law KY (2011) Study of wetting and adhesion interactions between water and various polymer and superhydrophobic surfaces. *J Phys Chem C* 115:14852–14861
27. Extrand CW, Kumaga Y (1995) Liquid drops on an inclined plane. The relationship between contact angles, drop shape, and retention force. *J Colloid Interface Sci* 170:515–521
28. Extrand CW, Gent AN (1990) Retention of liquid drops by solid surfaces. *J Colloid Interface Sci* 138:431–442
29. Furnidge CGL (1962) Studies at phase interfaces I. The sliding of liquid drops on solid surfaces and a theory for spray retention. *J Colloid Sci* 17:309–324
30. Macdougall G, Ockrent C (1942) Surface energy relations in liquid/solid systems. 1. The adhesion of liquids to solids and a new method of determining the surface tension of liquids. *Proc R Soc Lond A* 180:151–173
31. Antonini C, Carmona FJ, Pierce E, Marengo M, Amirfazli A (2009) General methodology for evaluating the adhesion force of drops and bubbles on solid surfaces. *Langmuir* 25:6143–6154
32. Pierce E, Carmona FJ, Amirfazli A (2008) Understanding of sliding and contact angle results in tilted plate experiments. *Colloids Surf A Physicochem Eng Asp* 323:73–82
33. Krasovitski B, Marmur A (2005) Drops down the hill: theoretical study of limiting contact angles and the hysteresis range on a tilted plate. *Langmuir* 21:3881–3885
34. ElSherbini AI, Jacobi AM (2004) Liquid drops on vertical and inclined surfaces 1. An experimental study of drop geometry. *J Colloid Interface Sci* 273:556–565
35. Della Volpe C, Siboni S, Morra M (2002) Comments on some recent papers on interfacial tension and contact angles. *Langmuir* 18:1441–1444
36. Cheng DF, Urata C, Masheder B, Hozumi A (2012) A physical approach to specifically improve the mobility of alkane liquid drops. *J Am Chem Soc* 134:10191–10199
37. Tadmor R, Bahadur P, Leh A, N'guessan HE, Jaini R, Dang L (2009) Measurement of lateral adhesion forces at the interface between a liquid drop and a substrate. *Phys Rev Lett* 103:266101
38. Gao L, McCarthy TJ (2006) Contact angle hysteresis explained. *Langmuir* 22:6234–6237
39. McHale G, Shirtcliffe NJ, Newton MI (2004) Contact angle hysteresis on superhydrophobic surfaces. *Langmuir* 20:10146–10149
40. Pease DC (1945) The significance of the contact angle in relation to the solid surface. *J Phys Chem* 49:107–110
41. Johnson RE, Dettre RH (1964) Contact angle hysteresis 1. Study of an idealized rough surface. In: Fowkes F (ed) Contact angle, wettability, and adhesion, advances in chemistry. American Chemical Society, Washington, DC, pp 112–135
42. Neumann AW, Good RJ (1972) Thermodynamic of contact angles 1. Heterogeneous solid surfaces. *J Colloid Interface Sci* 38:341–358

43. Wenzel RN (1936) Resistance of solid surfaces to wetting by water. *Ind Eng Chem* 28:988–994
44. Forsberg PSH, Priest C, Brinkmann M, Sedev R, Ralston J (2010) Contact line pinning on microstructured surfaces for liquids in the Wenzel state. *Langmuir* 26:860–865
45. Extrand CW (2002) Model for contact angles and hysteresis on rough and ultraphobic surfaces. *Langmuir* 18:7991–7999
46. Bartell FE, Bjorklund CW (1952) Hysteresis of contact angles. A study of interfacial contact angles in the mercury-benzene-water system. *J Phys Chem* 56:453–457
47. Chen YL, Helm CA, Israelachville JN (1991) Molecular mechanisms associated with adhesion and contact angle hysteresis of monolayer surfaces. *J Phys Chem* 95:10736–10747
48. Holly FJ, Refojo MF (1975) Wettability of hydrogels 1. Poly(2-hydroxyethyl methacrylate). *J Biomed Mater Res* 9:315–326
49. Lee S, Park JS, Lee TR (2008) The wettability of fluoropolymer surfaces: influence of surface dipoles. *Langmuir* 24:4817–4826
50. Extrand CW, Kumagai Y (1997) An experimental study of contact angle hysteresis. *J Colloid Interface Sci* 191:378–383
51. Zhao H, Park CK, Law KY (2012) Effect of surface texturing on superoleophobicity, contact angle hysteresis and “robustness”. *Langmuir* 28:14925–14934
52. Nosonovsky M (2007) Model for solid–liquid and solid–solid friction of rough surfaces with adhesion hysteresis. *J Chem Phys* 126:224701
53. Kanungo M, Mettu S, Law KY, Daniel S (2014) Effect of roughness geometry on wetting and de-wetting of PDMS surfaces. *Langmuir* 30:7358–7368
54. Law JBK, Ng AMH, He AY, Low HY (2014) Bioinspired ultrahigh water pinning nanostructures. *Langmuir* 30:325–331
55. Mettu S, Kanungo M, Law KY (2013) Anomalous thermally induced pinning of a liquid drop on a solid substrate. *Langmuir* 29:10665–10673
56. Koch K, Barehloft W (2009) Superhydrophobic and superhydrophilic plant surfaces: an inspiration for biomimetic materials. *Philos Trans R Soc A Math Phys Eng Sci* 367:1487–1509
57. Zhao H, Law KY, Sambhy V (2011) Fabrication, surface properties, and origin of superoleophobicity for a model textured surface. *Langmuir* 27:5927–5935
58. Krumpfer JW, McCarthy TJ (2010) Contact angle hysteresis. A different view and a trivial recipe for low hysteresis hydrophobic surfaces. *Faraday Discuss* 146:103–111
59. Sambhy V, Law KY, Zhao H, Chugh S (2013) Thermally stable oleophobic low adhesion coating for inkjet printing front face. US Patent 8,544,987
60. Urata C, Cheng DF, Mashedor B, Hozumi A (2012) Smooth, transparent and non-perfluorinated surfaces exhibiting unusual contact angle behavior towards organic liquids. *RSC Adv* 2:9805–9808
61. Kovacs GJ, Law KY, Zhao H, Sambhy V (2012) Coating for an ink jet printhead front face. U.S. Patent 8,226,207